Article

Journal of Advanced Electrochemical Storage

www.pubj.org

Investigation of magnetic and structural properties on Cobalt doped Barium Ferrite via Co-precipitation Method

S. Vadivelan[1,*], S.Sowmiya[2]

[1,*]Department of physics, Karpaga Vinayaga College of Engineering and Technology, Chengalpattu - 603305, Tamil Nadu, India.

[2]Department of physics, SRM Valliammai Engineering College, Kattankulathur- 603203, Tamil Nadu, India.

Cite This: *J. Adv. Electro. Storage* 2025, 1, 30–43

ABSTRACT: In this paper, it is planned to synthesize the cobalt doped barium ferrite using co-precipitation technique at different ratios. This is done in order to avoid the magnetic loss and increasing the permeability of this material. The different ratio (0-8%) of cobalt doped barium ferrite samples are exposed to sintering process under the temperature 1200°C for 6 hrs and the X-ray powder diffraction analysis is carried out. The analysis designates that the measured values agree to the standard parameters (a=b=5.864 Å, and c=23.099 Å), approving that the samples belong to the system is hexagonal. By using beam of X-rays, XPS spectrums are obtained, and the binding energy of the sample is measured. The vibrating sample magnetometer (VSM) measures the magnetic saturation, magnetic remanance and coercivity of a sample. The magnetic saturation, magnetic remanence and coercivity values are found and tabulated.

Keywords

Magnetic materials, saturation magnetization, coercivity, ferrites.

1. INTRODUCTION

The apprehension Barium ferrite is a material with strong magnetic properties and a high packing density. It is commonly used in magnetic card strips, speakers, and magnetic tapes due to its magnetic qualities and resistance to temperature, corrosion, and oxidation. Recent advancements have been directed toward exploring barium ferrite for long-term data storage solutions [1, 2]. The material has also proven to be resistant to a number of different environmental stresses, including humidity and corrosion. As the ferrites are already oxidized it cannot be oxidized any further. This is one reason for ferrites being so resistant to corrosion and also proved to be resistant to thermal demagnetization. As the high intrinsic coercivity enhances, making them more resistant to thermal demagnetization at the temperature of barium ferrite magnets rises [3, 4]. This characteristic of barium ferrite makes it as the most opted material in motor and generator designs and also in loudspeaker applications.

Ferrite magnets are extremely good insulators; hence they don't allow any electrical current to flow through them. They are also brittle as it is one of the ceramic characteristics. Ferrite magnets also have good machining properties, which allow the material to be cut into many shapes and sizes [5, 6]. Barium ferrites are corrosion-resistant and generally stable to

moisture and these ferrite particles have been used to store data on tapes and magnetic strips, but they have reached their limit for high capacity data storage A thicker passivation coating becomes necessary to prevent the oxidation and degradation of the barium ferrite particles at reduces in size. Barium ferrite completely out classes metal particles, mostly because it is already in its oxidized state and hence its size cannot be restricted by a protective coating. Compared to the unorganized rod like metal particles, it is easy to organize barium ferrite, due to its hexagonal pattern [7].

The material is seen around the world in applications such recording items like tapes and other applications in media devices, permanent magnets, and magnetic stripe cards (such as credit cards, hotel keys, and ID cards) [8, 9]. The material's stability allows for significant size reduction, leading to a much higher packing density. Barium ferrite, which has recently replaced the oxide, achieves much greater coercivity levels, which render the material magnetically hard, thus enhancing its suitability for recording materials. As discussed earlier, the ID cards and their readers are implanted with a unique pattern of Barium ferrite. The scanner is able to identify the card by the small reader that is implanted with the magnetic barium ferrite pattern, and this recognizes the pattern that is also found in the cards' barcode [10-12]. The materials can be formed into almost any shape and size using a process called sintering, whereby powdered barium ferrite is pressed into a mold, and then heated until it fuses together. The barium ferrite turns into a solid block without losing its magnetic properties. The magnets have an excellent resistance to demagnetization which has allowed them to be useful in speaker units over a long period of time.

Barium ferrite has been found to be a unique storage medium for Linear Tape-Open (LTO) storage and plays an important role in shaping the future of LTO tapes because of its high packing density [13-14]. The increase in packing density leads to a corresponding rise in the recording area. This stands in stark contrast to metal particle technology, which has started to fade away because of problems shrinking the particles past 100 nm. Barium ferrite can be reduced to a much smaller size and can be stacked a lot better because of its greater packing density and hexagonal structure. The aim of introducing divalent cations such as cobalt into barium ferrite is to increase its coercivity. From the magnetic characterization, the above statement is proved with the help of VSM characterization [15, 16]. The focal aspire of this work was to make the grade of some amalgamation variables on the magnetic properties of barium ferrite produced by co-precipitation technique is used to increase the storage capacity. The important factor of this method is fine particles are obtained from this homogeneous reaction. From the reaction excellent reactivity powder were produced to agree the decrease in sintering temperature. Compared to other preparation techniques, the co-precipitation technique produces results that are very clear, accurate and cost effective.

2. EXPERIMENTAL

2.1 Material preparation

The cobalt doped and undoped barium ferrite powder materials were prepared by co-precipitation method. Purified barium nitrate (Ba

$(NO_3)_2$), ferric nitrate (Fe $(NO_3)_3$), cobalt nitrate (Co $(NO_3)_2$), citric acid ($C_6H_8O_7$) and ammonium hydroxide (NH_4OH) were purchased from scientific material and technology The stoichiometric amounts of barium nitrate (Ba (NO_3)) $_2$, ferric nitrate (Fe $(NO_3)_3$) and cobalt nitrate ((Co $(NO_3)_2$) were mixed in ammonium hydroxide (NH_4OH) with distilled water and citric acid ($C_6H_8O_7$). citric acid is used to obtain the clear product. The synthesizing process is totally controlled by ammonium hydroxide to produce various doping percentages ofcobalt nitrate by co-precipitation method. The precipitated materials were collected by filtration method and wash away 4 times with distilled water. The final precipitate material is sent to drying process at 80°C for 6 hours. The dried material is ground to powder and allowed to undergo sintering process at 1200°C for 6 hrs. Finally, the cobalt doped barium ferrite composition ($BaCo_xFe_{12-x}O_{19}$) is obtained by this technique.

2.2 MATERIALS CHARACTERIZATION

The crystal structure of the synthesized ferrite powders is identified by X-ray measurements of Bruker D2 Phaser Powder X-ray diffractometry using CuK_α radiation ($\lambda = 1.541$ Å) in the range of 10º to 80º. Thermogravimetry / differential thermal analysis is performed on the sample materials using a Netzsch STA 409, over the temperature range of 20–1200°C at a rate of 20°C /min. Formation of pure and doped cobalt ferrite is also analyzed by FTIR Spectrophotometer of BRUKER ALPHA using opus 6.5 (version) software. The oxidation states of these samples were obtained from X-Ray Photoelectron Spectroscopy (XPS) using Kratos Analytical Axis Ultra DLD with aluminum anode as source operating at 160 eV pass energy, the morphology of the samples are analyzed by scanning electron microscope (SEM) VEGA3 TESCAN. The magnetic properties of the samples were characterized by vibrating sample magnetometer (VSM) Lakeshore (7410) at room temperature with an applied magnetic field of 20 kOe.

3. RESULTS

3.1 THERMAL ANALYSIS

This analysis used to determine the characteristics of materials that exhibit either mass loss or gain due to decomposition and oxidation process. From TG/DTA, the degradation mechanisms, reaction kinetics, determination of organic content and determination of inorganic (e.g. ash) content in a sample are analyzed [17, 18]. The Fig. 1 shows the TG/DTA plots for the compound containing a mixture of $BaCo_3$, Fe_2O_3 and doping weight % of Co $(NO_3)_2$is 0%, 2%, 4%, 6%, and 8% respectively. The weight loss is incremental and an overall loss of about 4% is indicated. There is an exterior of an endothermic peak in the DTA curve at 848°C.

The peak is attributed to the decarboxilation of $BaCO_3$, reported to take place at 1000°C for pure carbonate and around 800°C for the mixture of carbonate and iron oxide [19, 20]. The completion of the formation of barium ferrite is indicated at around 1010°C to 1090°C. The exothermic DTA curve indicates that residual of Co_3O_4 to Co_2O_3 transformation occurred at the temperature 580°C.It is to be noted here that the conversion is very fast and is displayed by the appearance of a sharp spike coupled with the endothermic reaction [21, 22]. The rapid exothermic response at the start of the trace may also be due to the elasticity effect.

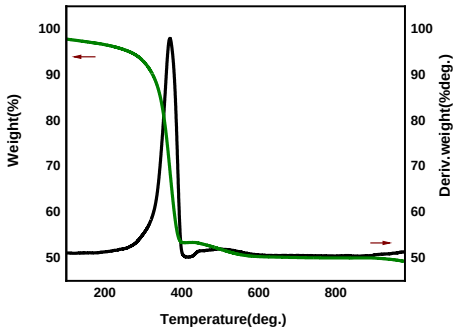

Figure 1 DTA/ TGA pattern for pure barium ferrite

3.2 XRD ANALYSIS

X-ray diffraction pattern The X-ray diffraction patterns for both the pure and cobalt-doped $BaFe_{12}O_{19}$ compounds are illustrated in Fig. 2. The XRD characteristic peaks confirm that the crystal structure is hexagonal, in accordance with JCPDS 78-0133. The strong diffraction peaks of pure and cobalt doped $BaFe_{12}O_{19}$ samples exhibit standard peaks at 2θ values corresponding to (110), (107) and (114) planes respectively [23-25]. The absence of any other peaks (apart from $BaFe_{12}O_{19}$ peaks) in the XRD pattern indicates the spotlessness of the synthesized samples.

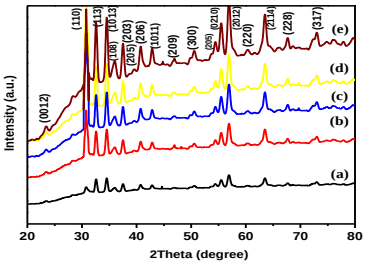

Figure 2 XRD pattern of the samples: (a) Pure nano barium ferrite and (b) Co-2mol %, (c) Co-4mol %, (d) Co-6mol %, (e) Co-8mol % doped nano barium ferrite

The broadening of the peaks indicates an increase from surface to volume ratio and decrease in the diameter of the particles. From the Scherrer formula [26-28] the average crystallite sizes (t) of the prepared ferrite samples were determined.

$$t = \left(\frac{k\lambda}{\beta\cos\theta}\right) \qquad (1)$$

Where k denotes the Scherrer constant (k=0.89), λ is the wavelength of X-ray radiation (λ=1.54 Å), β is the full width half maximum of the diffraction peak and θ is the diffraction angle. The crystallite size (t) of the samples under investigation as quit from single-line approach of the XRD reflections are tabulated in Table 1. From the table it is found that the crystallite size of pure barium ferrite is 36.8 nm, while different ratio of Co^{2+} doping in the barium ferrite, the crystallite size is reduced. Thus, it can be concluded that the crystallite size strongly depends on Co^{2+} concentration which impede the grain growth, thereby making the crystallite size. The crystallite size (t) of the samples under investigation as quit from single-line approach of the XRD reflections are tabulated in Table 1. From the table it is found that the crystallite size of pure barium ferrite is 36.8 nm, while different ratio of Co^{2+} doping in the barium ferrite, the crystallite size is reduced. Thus, it can be concluded that the crystallite size strongly depends on Co^{2+} concentration which impede the grain growth, thereby making the crystallite size to decrease with its increasing concentration [29, 30]. Table 1 show that the elastic strain value is

increased with increasing Co^{2+} concentration. It reveals that the possible growth of cobalt ferrite particles with larger defects in this favored direction; switch over to smaller crystallite size. The lattice constant (a) is calculated for all the compositions by using this relation [31],

$$\frac{1}{d^2} = \frac{4}{3}\left[\frac{h^2+hk+k^2}{a^2}\right] + \frac{l^2}{c^2} \quad (2)$$

Where d is the value of d-spacing of line in XRD pattern and (hkl) are the Miller indices. Table 1 lists the calculated values of lattice constant of all the prepared samples with efficiency of ±0.003 Å. From the table, it is found that the lattice constant (a) increased with increase in the Co^{2+} concentration and also increases the specific surface area of the particles. The elastic strains of the samples are also calculated by the given expression [32],

$$\varepsilon = \frac{\beta}{2\cot(\theta)} \quad (3)$$

The elastic constant values are indexed in Table 1.The Co^{2+} concentration is found to beincreasing with an increase in the elastic constant value of the samples. From the Williamson and Hall methodthe average crystallite size and strain induced by the doped Co^{2+} concentration was calculated using below the expression [33],

$$\beta_{(hkl)}\cos\theta_{(hkl)} = \frac{K\lambda}{D} + 4\varepsilon\sin\theta_{(hkl)} \quad (4)$$

Table 1 Summary of Pure and Co- doped nano barium ferrite Calcined at 1200 ° C

Composition / 1200° C	Crystalline size (nm)		Average crystalline size 't'(nm)	a (Å)	c (Å)	Volume $(Å)^3$	Elastic Strain ε (X 10^{-3})
	Scherrer method	W–H method					
Pure	33.5	35.9	34.70	5.86	23.09	688.11	3.73
2mol% Co	33.9	36.1	35.00	5.89	31.74	875.79	3.69
4mol% Co	35.3	36.8	36.05	5.89	31.84	876.82	3.82
6mol% Co	36.1	37.9	37.00	5.89	31.68	869.84	3.88
8mol% Co	36.9	39.1	38.00	5.89	31.76	863.76	3.93

Where K is a constant (0.89), λ is the wavelength of CuKα (1.5406 A °), D is the crystallite size in nanometers, β is the full width half maximum (FWHM) of XRD peak intensity, h is the peak position (Bragg angle) and ε is the micro strain. The Williamson–Hall plot has been made between $\beta_{(hkl)}\cos\theta$ and $4\sin\theta_{(hkl)}$ whereas the slope line corresponds to strain as shown in Fig. 3.

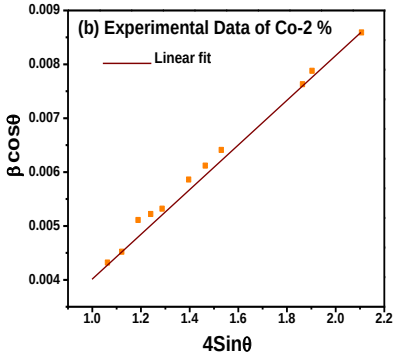

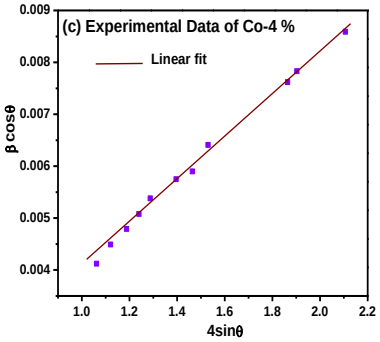

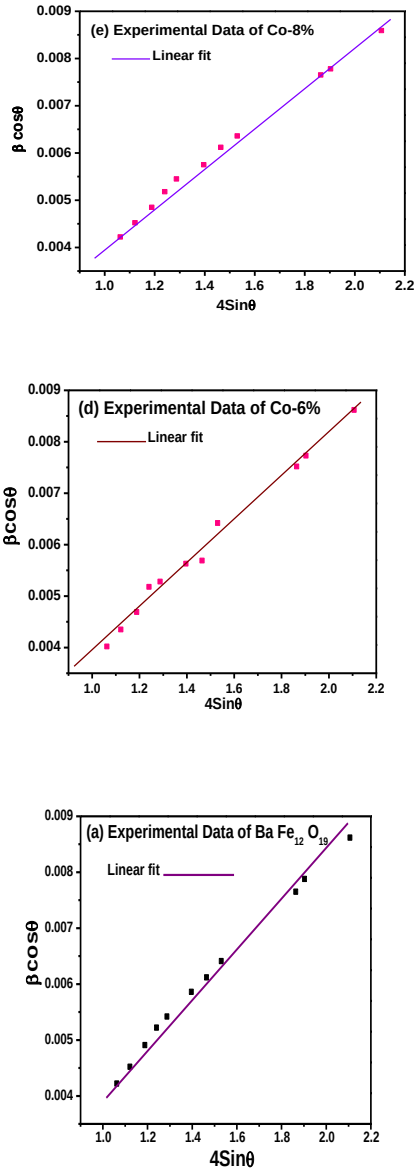

Figure 3 Williamson–Hall plots of the samples: (a) Pure nano barium ferriteand (b) Co-2mol %, (c) Co-4mol %, (d) Co-6mol % (e) Co-8mol % doped nano barium ferrite

3.3 FT-IR Analysis

FTIR spectrum analysis has been used to find the information about chemical bonding in a compound. The absorption peaks purely depend on the crystal structure, morphology and chemical composition of the materials in order to determine the chemical bonding nature of pure and cobalt doped barium ferrite compound [34, 35]. The Fig. 4 shows that the FT-IR spectra of barium ferrite are recorded in the range 400–4000 cm–1 wave numbers. The intense absorption band appeared between the frequencies regions of 400–1000 cm-1, characterizes the deformation modes of Co–O and Fe–O. In addition, the absorption band below 500 cm–1 is due to the deformation of Fe–O bonds in the deformation of Fe–O–Fe bridges [36, 37].

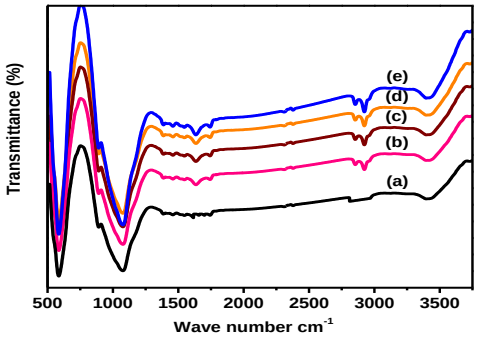

Figure 4 FT-IR pattern of the samples: (a) Pure nano barium ferriteand (b) Co-2mol %, (c) Co-4mol %, (d) Co-6mol %, (e) Co-8mol % doped barium nanoferrite.

The strong absorption peak around 805 cm^{-1} is associated with O–Fe–O vibration mode. Further, the absorption band in the region of 3200–3500 cm^{-1} corresponds to OH stretching vibration of water molecules absorbed over the surface of the samples and the absorption peak is located about 1571 cm^{-1} corresponding to bending mode of H–O–H [38, 39]. The conditional absorption of CO_2 over the surface of prepared samples from the atmosphere was identified from the sharp peak positioned about 2339 cm^{-1}. From the

spectra, the O–C–O stretching band at 2347 cm^{-1} is identified due to an increase in doped concentration of cobalt nitrate [40]. Hence, the observed metal oxide vibrations in the frequency range of 400–4000 cm^{-1} reveal the material phase and chemical purity of all the pure and Co^{2+} doped $BaFe_{12}O_{19}$ compounds.

3.4 XPS ANALYSIS

Chemical states and Surface analysis of the synthesized sample were investigated by X-Ray photoelectron spectroscopy (XPS). Fig. 5 shows the XPS wide spectrum of cobalt doped barium ferrite synthesized by co-precipitated technique. The photoelectron peaks of Co 2p, Fe 2p and O 1s along with C 1s were observed in this spectrum [41]. The fig. 6a shows that, the Ba 3*d*5/2 and Ba 3*d*3/2 peaks are observed at 780.748 and 784.429eV respectively, which are used to characterize the sample. The spectrum indicates a slight shift in the binding energy of the Ba peak in the ferrite material compared to that in BaO, primarily due to the varying environments of the Ba2+ ion within the compounds.

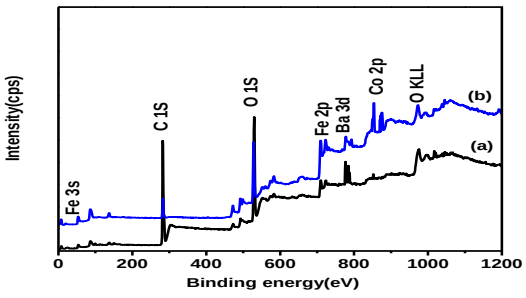

Figure 5 XPS spectrum: (a) pure nano barium ferriteand (b) Co-2mol % doped nano barium ferrite

Fig. 6b exhibitions the XPS bands of the co-doped ferrite, showing peaks for Co 2p3/2 and Co 2p1/2 at binding energy values of 853.05 eV and 872.732 eV, respectively. These peaks are conformed the Co^{2+} ion present in the cobalt ferrite particles [42, 43]. Fig. 6c shows the Fe 2p core shell XPS spectra of cobalt ferrite. This result is in close agreement with previous literature for Fe^{3+} ion in ferrite materials. Significantly, the high resolution XPS spectra of Fe 2p is shown in Fig. 6c can be fitted into two distinct peaks located at 723.573 eV and 726.858 ev.

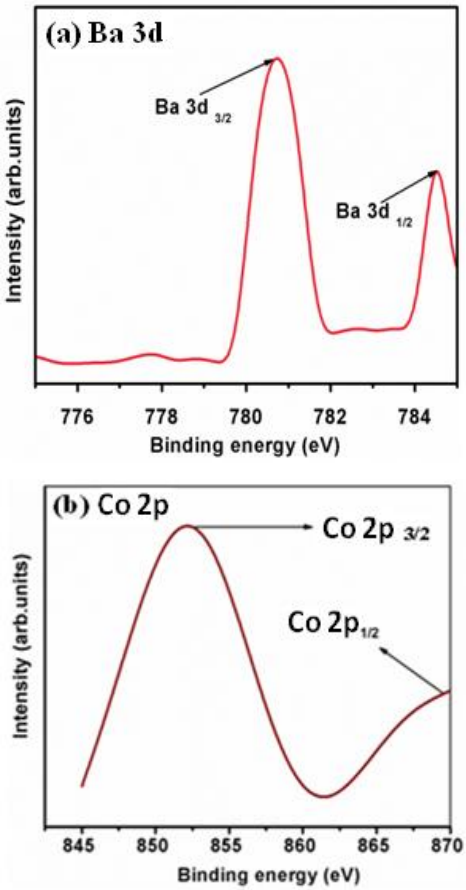

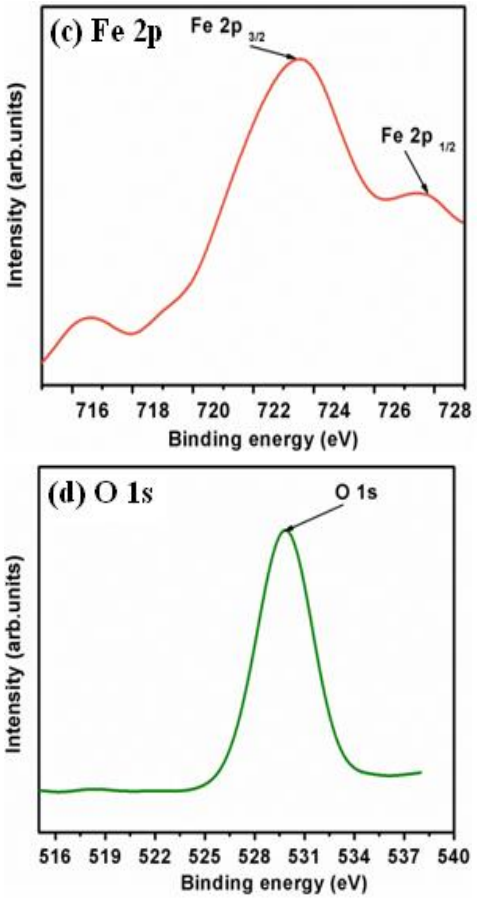

Figure 6 XPS high resolution spectrum: (a) Ba 3d, (b) Co 2p, (c) Fe 2p and (d) O1s

These peaks correspond to the binding energies of Fe 2p3/2-Fe^{2+} and Fe 2p3/2-Fe^{3+} ions. Therefore, the oxidation states of iron (Fe) in the prepared nanoparticles definitely consists of both Fe^{3+} and Fe^{2+} ions [44-46]. From the XPS spectra of the O 1s region was found at 531.123 eV, as shown in Fig. 6d. This peak is associated with corresponding binding energy of O^{2-} metal group observed from the surface of the sample.

3.5. SCANING ELECTRON MICROSCOPE (SEM)

The SEM image of the pure and Co^{2+} doped barium ferrite synthesized by a chemical co-precipitation technique at sintered temperature 1150°C as shown in Fig. 7.

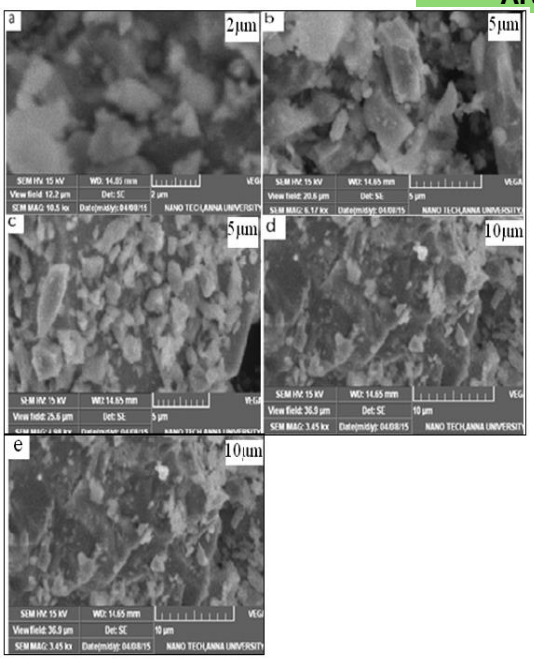

Figure 7 SEM image of the samples: (a) Pure nano barium ferriteand (b) Co-2mol % , (c) Co-4mol % , (d) Co-6mol % , (e) Co-8mol % doped barium nanoferrite

From the SEM image that the grains are non-uniform and densely distributed on the surface, more over the grain size of the ferrite found to be in the range of 50µm -2µm [47-49]. The images show that the grain size of the samples decreased as well as increased the percentage of Co^{2+}.

3.6 VIBRATING SAMPLE MAGNETOMETER ANALYSIS (VSM)

The vibrating sample magnetometer measures the magnetic saturation and coercivity value of a sample of magnetic material is placed in an external magnetic field by converting the dipole field of the sample into an ac electrical signal [50, 51]. From the analysis, the pure and Co^{2+} doped (x=0%, 2%, 4%, 6% and 8%) barium ferrite

hysteresis loops are shown in Fig. 8. The magnetic measurements of the data are summarized in Table 2. After doping, the observed saturation magnetization (Ms) decreasesfrom 58.753 to57.968 emu/g with increase in the cobalt percentage.The saturation magnetization (Ms) value of pure barium ferrite is 58.753emu/g at 300K. From the hysteresis loop, the remnant magnetization (Mr) of the pure and Co^{2+} doped

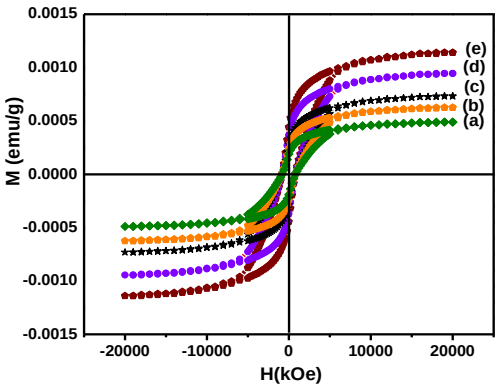

Figure 8 Hysteresis pattern for the samples: (a) Pure nano barium ferriteand (b) Co-2mol %, (c) Co-4mol %, (d) Co-6mol %, (e) Co-8mol % doped barium nanoferrite

barium ferrite are decreases with increase in doped percentage of Co^{2+} [52, 53]. The remnant magnetization (Mr) at 300K for pure and Co^{2+} doped barium ferrite is 15.234 emu /g and 17.986 emu /g -7.758 emu /g.The squareness (SQR) value of these samples is calculated by this ratio (Mr/ Ms). In general, large SQR values are favored in many magnetic storage applications. The SQR value decreases with increasing doped percentage of Co^{2+} [54, 55]. The SQR value of the pure barium ferrite sample at 300 K is 0.2592 and doped percentage of Co^{2+} increased thereby decreasing the SQR value simultaneously.

Table 2 Summary of pure and Co- doped nanobarium ferrite Calcined at 1200 ° C

Composition / 12 C	Ms (Saturation magnetization) (emu/g)	Mr (Remnant magnetization) (emu/g)	(Mr/Ms) ratio	Hc (Coercivity) (Oe)
Pure	11.7	4.09	0.34	851.12
2mol% Co	24.8	8.87	0.35	851.15
4mol% Co	28.5	11.12	0.39	853.16
6mol% Co	31.2	13.1	0.41	854.79
8mol% Co	34.5	26.2	0.75	856.32

From the hysteresis loop, the SQR value of 8% cobalt doping is calculated as 0.1347 at 300 K. However, the SQR values depend on the doping percentage of Co^{2+}.The coercivity value for pure barium ferrite is 851.128 Oe at 300K. In addition the cobalt doping percentage (2-8%) increased with varying the coercivity values (998.584 Oe -213.564 Oe). After doping, the observed Msvalue decreasesfrom 58.687emu/g to 57.968emu/g with increase in the Co^{2+} doped percentage [56]. From the data, SQR value is obtained as dependency of the Co^{2+} doped percentage. SQR and coercivity value is varied from the prepared sample density.

4. CONCLUSION

The various ratio of Co^{2+} doped barium ferrite with sintering temperature 1200°C which it's involved the various characterization have

been discussed above. TGA/DTA result explains completion of the formation of barium ferrite at the temperature around 1010°C to 1100°C. From the XRD studies, the 0%, 2%, 4%, 6%, and 8%of Co^{2+} doped barium ferrite confirms the hexagonal structure. The functional groups exhibited in barium ferrite structure were investigated by FT-IR spectroscopy and the resultant spectra are presented clearly. The surface phenomenon and oxidation state were characterized by XPS technique. Detailed surface analysis of core level spectra of Co 2p, Fe 2p, Ba 3d and O 1s peak were studied and found to be 2^+ state for cobalt and 3^+ states for iron on the surface of prepared samples. The SEM images show the size of the pure and Co^{2+} dopedbarium ferrite samples in the range of micro meter (50 μm -2μm).

From the magnetization studies, the saturation magnetization Ms Value is decreased by increasing Co^{2+} doped barium ferrite from 0-8% is 58.753 emu/g to57.968 emu/g and remnant magnetization Mr is decreased from 15.234 emu/g to7.758 emu/g with 0-8% of Co^{2+} doped barium ferrite. The coercivity Hc is decreased from 851.128 Oe to 213.564 Oe for increasing the Co^{2+} doped percentage from 0 to 8 % respectively at 300K. It was observed that the magnetic property is very close to temperature dependency. From the Mr and Msvalue, the SQR is calculated. SQR (squareness) and coercivity also depend on the density of the percentage of Co^{2+} doping. During the preparation and sintering process, the magnetic properties of the samples are affected prominently.

REFERENCE

[1] Sozeri, H. Kucuk, L. Ozkan, H. Improvement in magnetic properties of La substituted $BaFe_{12}O_{19}$ particles prepared with an unusually low Fe/Ba molar ratio, Journal of Magnetism and Magnetic Materials 323 (2011) 1799-1804

[2] Salvi, S.V. Joshi, V.H. Effect of PH on magnetic properties of doped barium hexaferrite, Indian Journal of Pure & Applied Physics 4 (2009) 277-281.

[3] Gubin, S.P. Koksharov Yu, A. Khomutov, G.B. YurkovYu,G. Magnetic nanoparticles: preparation, structure and properties, Russian Chemical review 74 (2005) 489-520.

[4] Murthy, Y.L.N. Kasiviswanath, I.V. Synthesis and characterization of nickel copper ferrite, International Journal of ChemTech Research 1 (2009) 1308-1314.

[5] Hessien, M. Rash ad, M. El-Barawy, K. Controlling the composition and magnetic properties of strontium hexaferrite synthesized by co-precipitation method, J. Magn. Magn. Mater. 320 (2008) 336–343.

[6] Schloemann, E. Advances in ferrite microwave materials and devices, J. Magn. Magn. Mater. 209 (2000) 15-20.

[7] Altenburg, H. Plewa, J. Plesch, G. Shpotyuk, O. Influence of the agglomeration in the initial suspension (ferrofluid) on the oriented magnetic structure, Pure Appl. Chem. 74 (2002) 2085-2093.

[8] Biest, O. VandeperreAnnu, L. Electrophoretic deposition of materials, Rev. Mater. Sci. 29 (1999) 327-352.

[9] Carp, O. Barjega, R. Segal, E. Brezeanu, M. Nonco-nventional methods for obtaining hexaferrites,ThermochimicaActa, 318 (1998) 57-63.

[10] Garcia-Casillas, P.E. Beesley, A.M. Bueno, D. Martinez, C.A. Remanence properties of barium

hexaferrite, Journal of Alloys and Compounds 369 (2004) 185-196.

[11] Makled, M.H. Matsui, T. Tsuda, H. Mabuchi, H. El- Mansy, M.K. Infrared Spectroscopy and Thermal Stability Studies of Natural Rubber-Barium Ferrite Composites, Journal of Materials Processing Technology 160 (2005) 229-233.

[12] Golosovsky, M. Saado, Y. Davidov, D. Self-assembly of floating magnetic particles into ordered structures: A promising route for the fabrication of tunable photonic band gap materials, Applied Physics Letters 7 (1999) 4168-4175.

[13] Hur, N.H. Park, J.Y. Dho, Kim, S.J. Lee, E.K. Magnetic and microstructural properties on Mn- and Ru-doped hexagonal barium ferrites, IEEE Trans. Magn. 40 (2004) 2790–2792.

[14] Singh,P. Babbar, V.k. Razdan, A. Srivastava, S.L. Agrawal, V.K. Goel, T.C. Dielectric constant, magnetic permeability and microwave absorption studies of hot-pressed Ba-Co Ti hexaferrite composites in X-band, J. Mater. Sci. 41 (2006) 7190–7196.

[15] Shams, N. Liu, X. Matsumoto, M. Morisako, A. Microstructure and magnetic properties of commercial barium ferrite powders, Journal of Magnetism and Magnetic Materials 290 (2005) 138-140.

[16] Dobrzaski, L.A. Drak, M. Zibowicz, B.Materials with specific magnetic properties, Journal of Achievements in Materials and Manufacturing Engineering 17 (2006) 37-43.

[17] Zibowicz, B. Szewieczek, D. Dobrzaski, L.A. New possibilities of application of composite materials with soft magnetic properties, Journal of Achievements in Materials and Manufacturing Engineering 20 (2007) 207-217.

[18] Qiu, J. Gu, M.Magnetic nanocomposite thin films of $BaFe_{12}O_{19}$ and TiO_2 prepared by sol–gel method, Applied Surface Science 252 (2005) 888-892.

[19] Mali, A. Ataie, A.Structural characterization of nano-crystalline $BaFe_{12}O_{19}$ powders synthesized by sol–gel combustion route, ScriptaMaterialia 53 (2005) 1065-1070.

[20] Drak, M. Dobrzaski, L.A.Corrosion of Nd-Fe-B permanent magnets, Journal of Achievements in Materials and Manufacturing Engineering 20 (2007) 239-242.

[21] Ding, J. Miao, W.F. McCormick, P.G. Street, R. High-coercivity ferrite magnets prepared by mechanical alloying, Journal of Alloys and Compounds 281 (1998) 32-36.

[22] Temuujin, J. Aoyama, M. Senna, M. Masuko, T. Ando, C. Kishi, H. Synthesis of Y-type hexaferrites via a soft mechanochemical route, J. Solid State Chem. 177 (2004) 3903-3908.

[23] Vadivelan, S. Victorjaya, N. Investigation of Structural, Thermal and Magnetic properties of Strontium substituted Barium Hexaferrite Synthesized via co-precipitation Method, International Journal of ChemTech Research 8 (2015) 404-410.

[24] Prasad, N.K. Naulakha, A. Jha, N. Meena, S.S. Bahadur, D. Prakash, O. Mandal, R.K.Magnetic and electric properties of nanoparticles of Ni-substituted ferrites synthesized using a microwave refluxing process, Int. J.Mater.Res.104 (2012) 680-685.

[25] Singhal, S. A comparative study on the magnetic properties of $MFe_{12}O_{19}$ and $MA_lFe_{11}O_{19}$ (MQSr, Ba and Pb) hexaferrites with different morphologies, Ceram. Int. 37 (2011) 1833–1837.

[26] Q. Xing, Q. Peng, Z. Wanga, C.B. Fu Z. Fu, X. Structural, electrical and dielectric properties of

yttrium substituted nickel ferrites, Physica B407 (2012) 388-395.

[27] Ishaque, M. Islam, M.U. Azhar Khan, M. Rahman, I.Z. Genson A. Hampshire, S. Microstructure and Microwave Absorption Properties of Y-Substituted Ni-Zn Ferrites, Physica B. 405 (2010) 1532-1540.

[28] Haralkar, S.J. Kadam, R.K. More, S.S. SagarE.Shirsath, Mane, M.L. SwatiPatil Mane, D.R. Substitution effect of Cr3þ ions on the properties of Mg–Zn ferrite nanoparticles, Physica B 407 (2012) 4338–4346.

[29] Tholkappiyan, R. Vishista, K. N-N-methylene bis acrylamide: A novel fuel for combustion synthesis of zinc ferrite nanoparticles and studied by X-Ray photoelectron spectroscopy, International Journal of ChemTech Research6 (2014) 2834-2842.

[30] Nowosielski, R. Babilas, R. Dercz, G. Pajqk L. Wrona, J. Barium ferrite prepared by milling and annealing, Archives of materials science and engineering 22 (2007) 45-48.

[31] Drofenik, M. The hydrothermal synthesis of super-paramagnetic barium hexaferrite particles, Mater.Chem.Phys.127 (2011) 415–419.

[32] Patange, S.M. Shirsath, S.E. Toksha, B.G. Jadhav S.S. Jadhav, K.M. Electrical and magnetic properties of Cr3þ substituted nanocrystalline nickel ferrite, Journal of Applied Physics 106 (2009) 023914.

[33] Asghar, G. Anis-ur-Rehman, M. Structural, dielectric and magnetic properties of Cr–Zn doped strontium hexa-ferrites for high frequency applications, J. Alloys Compound 526 (2012) 85-90.

[34] Iqbal, M.J. Ashiq, M.N. Physical and electrical properties of Zr–Cu substituted strontium hexaferrite nanoparticles synthesized by co precipitation method, Chem. Eng. J. 136 (2008) 383.

[35] Kajal K MallickMagnetic properties of cobalt substituted M-type barium hexaferrite prepared by co precipitation, Journal of Magnetism and Magnetic Materials312 (2007) 418-429.

[36] Khademi, F. Structural, magnetic and microwave properties of Eu-doped barium hexaferrite powders, J. Supercond. Novel Magn. 25 (2012) 525–531.

[37] Hakola, A. Heczko, O. Jaakkola, A. Kajava, T. Ullakko, K. Pulsed laser deposition of NiMnGa thin films on silicon, Applied physics A 79 (2004) 1505-1508.

[38] Zhang, J.M. Zhang, Y. Xu, K.W. Ji, V. General Compliance Transformation Relation and Applications for Anisotropic Hexagonal, Metals Solid State Communications139 (2006) 87-91.

[39] Pramanik, N.C. Fujii, T. Nakanishi, M. Takada, J. Seok, S.I. The effect of heat treatment temperature on the microstructure and magnetic properties of $Ba_2Co_2Fe_{12}O_{22}$ (Co_2Y) prepared by sol–gel method, MaterLett. 60 (2006) 2718-2722.

[40] Yogamalar, R. Srinivasan, R. Vinu, A. Ariga, K. Bose, A.C. X ray peak broadening analysis in ZnO nanoparticles, Solid State Commun. 149 (2009) 1919-1923.

[41] Zhong, W. Ding, W. Zhang, N. Hong, J. Yan, O. Du, Y. Key step in synthesis of ultrafine $BaFe_{12}O_{19}$ by sol-gel technique,J. Magn Mater 168 (1997) 196-202.

[42] Jun Li Zhang Structural and Magnetic Behavior of Cobalt Doped $Ba_{0.5}Sr_{0.5}Fe_{12}O_{19}$ Nanoparticles Synthesized by Chemical Co-Precipitation Technique, Applied Mechanics and Materials 274 (2013) 406-410.

[43] Kim, S.G. Wang, W.N. Iwaki, T. Yabuki, A. Okuyama, K. Low-temperature crystallization of barium ferrite nanoparticles by a sodium citrate-aided synthetic process, J. Phys. Chem.*C*111 (2007) 10175–10180.

[44] Maensiri,S. Masingboon, C. Banjong, C. Seraphin, S. A simple route to synthesize nickel ferrite ($NiFe_2O_4$) nanoparticles using egg white, Scr. Mater. 56 (2007) 797–800.

[45] Nowosielski, R. Babilas, R. Dercz, G. Pajak, L. Microstructure of composite material with powders of barium ferrite, Journal of Achievements in Materials and Manufacturing Engineering 17 (2006) 117-120.

[46] Shepherd, P. Mallick, K. Green, R. Magnetic and structural properties of M-type barium hexaferrite prepared by coprecipitation, Journal of Magnetism and Magnetic Materials 311 (2007) 683–692.

[47] Mosleh, Z. Kamelin, P. Ranjbar, M. Salamati, H. Effect of annealing temperature on structural and magnetic properties of $BaFe_{12}O_{19}$hexaferrite nanoparticles, Ceramics International 40 (2014) 7279–7284.

[48] Jotania, B. Patel, A. Microstructure and Dielectric Properties of Mn Substituted $Sr_2Cu_2Fe_{12}O_{22}$ (Cu_2Y) Hexaferrite Powder, IJERA 2 (2012) 494-498.

[49] Zhao, Precursor-directed synthesis of quasi-spherical barium ferrite particles with good dispersion and magnetic properties, CrystEng Comm. 15 (2013) 808–815.

[50] Ravinder, D. Characterization of Co1-XZnxFe2o4 Nano Spinal Ferrites Prepared by Citrate Precursor Method, Int. Journal of Engineering Research and Applications 3 (2013) 654-660.

[51] Shobana, M.K. Calcium doped nickel ferrit powders prepared by sol-gel combustion method, International Journal of NanoDimension2 (2012) 275-279.

[52] Sharma, P. Rocha, R.A. De Medeiros, S.N. PaesanoJr, A. Structural and magnetic studies on barium hexaferrites prepared by mechanical alloying and conventional route, J. Alloys Comp 443 (2007) 37–42.

[53] TalwinderKaur, Srivastava, a.k. Effect of pH on Magnetic Properties of Doped Barium Hexaferrite, JRMET 3 (2013) 171-173.

[54] Lechevallier, L. Le Breton, J.M. Wang, J.F. Harris, I.R. Structural analysis of hydrothermally synthesized $Sr_{1-x}Sm_xFe_{12}O_{19}$ hexagonal ferrites, J. Magn. Magn.Mater. 269 (2004)192-196.

[55] Sandaranarayanan, VK, & Khan, D.C. 'Mechanism of the Formation of Nanoscale M-Type Barium Hexaferrite in the Citrate Precursor Method' , Journal of Magnetism and Magnetic Materials, 153 (1996), 337- 346.

[56] Schloemann, E 2000, 'Advances in ferrite microwave materials and devices', J. Magn. Magn. Mater., 209 (2000), 15-20.